Proceedings of the ASME 2021
15th International Conference on Energy Sustainability
ES2021
June 16-18, 2021, Virtual, USA

ES2021-60517

DRAFT: HEAT BASED POWER AUGMENTATION FOR MODULAR PUMPED HYDRO STORAGE IN SMART BUILDINGS OPERATION

Yang Chen*
Environmental Sciences Division
Oak Ridge National Laboratory
Oak Ridge, U.S.

Ahmad Abu-Heiba
Energy Science and Technology Directorate
Oak Ridge National Laboratory
Oak Ridge, U.S.

Saiid Kassaee
Department of Mechanical,
Aerospace, and Biomedical Engineering
University of Tennessee, Knoxville, U.S.

Chenang Liu
School of Industrial Engineering &
Management, Oklahoma State University
Stillwater, U.S.

Guodong Liu
Electrification and Energy Infrastructures Division
Oak Ridge National Laboratory
Oak Ridge, U.S.

Michael Starke
Electrification and Energy Infrastructures
Division, Oak Ridge National Laboratory
Oak Ridge, U.S.

Brennan T. Smith
Environmental Sciences Division
Oak Ridge National Laboratory
Oak Ridge, U.S.

Ayyoub M. Momen
Founder & CEO, Ultrasonic Technology Solutions
Energy Science and Technology Directorate
Oak Ridge National Laboratory
Oak Ridge, U.S.

ABSTRACT

In the U.S., building sector is responsible for around 40% of total energy consumption and contributes about 40% of carbon emissions since 2012. Within the past several years, various optimization models and control strategies have been studied to improve buildings energy efficiency and reduce operational expenses under the constraints of satisfying occupants' comfort requirements. However, the majority of these studies consider building electricity demand and thermal load being satisfied by unidirectional electricity flow from the power grid or on-site renewable energy generation to electrical and thermal home appliances. Opportunities for leveraging low grade heat for electricity have largely been overlooked due to impracticality at small scale. In 2016, a modular pumped hydro storage technology

*Corresponding Email: cheny2@ornl.gov. This manuscript has been authored in part by UT-Battelle, LLC, under contract DE-AC05-00OR22725 with the US Department of Energy (DOE). The US government retains and the publisher, by accepting the article for publication, acknowledges that the US government retains a nonexclusive, paid-up, irrevocable, worldwide license to publish or reproduce the published form of this manuscript, or allow others to do so, for US government purposes. DOE will provide public access to these results of federally sponsored research in accordance with the DOE Public Access Plan (http://energy.gov/downloads/doe-public-access-plan).

was invented in Oak Ridge National Laboratory, named Ground Level Integrated Diverse Energy Storage (GLIDES). In GLIDES, employing high efficiency hydraulic machinery instead of gas compressor/turbine, liquid is pumped to compress gas inside high-pressure vessel creating head on ground-level. This unique design eliminates the geographical limitation associated with existing state of the art energy storage technologies. It is easy to be scaled for building level, community level and grid level applications. Using this novel hydro-pneumatic storage technology, opportunities for leveraging low-grade heat in building can be economical. In this research, the potential of utilizing low-grade thermal energy to augment electricity generation of GLIDES is investigated. Since GLIDES relies on gas expansion in the discharge process and the gas temperature drops during this non-isothermal process, available thermal energy, e.g. from thermal storage, Combined Cooling, Heat and Power system (CCHP), can be utilized by GLIDES to counter the cooling effect of the expansion process and elevate the gas temperature and pressure and boost the roundtrip efficiency. Several groups of comparison experiments have been conducted and the experimental results show that a maximum 12.9% cost saving could be achieved with unlimited heat source for GLIDES, and a moderate 3.8% cost improvement can be expected when operated coordinately with CCHP and thermal energy storage in a smart building.

1. INTRODUCTION

In 2019, primary energy consumption of the United States was about 100.2 quadrillion British thermal Units, and for the first time since 1957, energy production exceeded energy consumption in the United States on an annual basis [1]. The production of petroleum and natural gas have both surpassed their previous highs set in 2018, while the renewable energy remained fairly constant by growing about 0.1 quad and nuclear electric power production has remained steady at nearly 8 quads for the past two decades. Coal power production has declined for the third year in a row and reached its lowest point since 1974. Among all the main energy-use sectors, building sector is responsible for 39% of total U.S. energy consumption in 2019, including 21% from residential sector and 18% from commercial sector. Generally, for buildings, The major areas of energy consumption in buildings are heating, ventilation, and air conditioning—35% of total building energy; lighting—11%; major appliances (water heating, refrigerators and freezers, dryers)—18% with the remaining 36% in miscellaneous areas including electronics [2]. Besides more strict building construction code and new advanced energy technology (e.g. more efficient heat pumps, electric storage, etc), large amount of research has been focused on integrated building system design and control strategies to achieve greater operation efficiency.

Upon satisfying thermal demand in buildings, combined cooling, heating and power system (CCHP) have been concerned widely in recent years as it could realize an energy cascade utilization with overall energy efficiency 90%, and is gradually replacing the conventional centralized energy supply to some extent [3]. The performance of CCHP system can be improved by integrating other energy sources [4], and thermal energy storage [5]. Shared with CCHP, thermal storage and battery, the collaborative decision model is developed to study energy exchange among two buildings under multi-objective framework [6]. A novel performance curve strategy is proposed to optimize CCHP operation [7], which leads to better performance than previously published operating strategies, such as following electrical load, following thermal load, following hybrid load, and matching performance strategies. Under these operation strategies, the performance of CCHP with cool thermal storage is evaluated for data center cooling energy supply [8]. To minimize fossil fuel consumption, a novel CCHP system including photovoltaic module, wind turbine and solid oxide fuel cells as prime movers is proposed [9], and then its feasibility is verified with battery and heat storage tanks based on the operation of a hypothetical hotel. A nonlinear, reduced order dynamic model is presented for a small scale combined heat and power system (CHP) with sensible thermal energy storage in the form of a stratified hot water tank [10]. The model's empirical parameters are identified and its accuracy is validated based on the experimental data from a micro-CHP testbed. In order to determine the optimal size of thermal energy storage and auxiliary boiler in micro-CHP system, the optimal behavior of different devices is predicted in in the design phase by developed mixed integer linear model, which can be useful in viability analysis. The modeling, planing and construction of large-scale seasonal hot-water thermal energy storage is discussed in [11] for renewable district heating. COMSOL Multiphysics software is used to develop both 2-D and 3-D thermal energy storage simulations, which are calibrated using measured data from pit thermal energy storage in Dronninglund (Denmark). The influence of thermal energy storage geometry on stratification quality is also investigated using a dimensionless indicator ranged in between perfectly-stratified tank (0) and a fully mixed tank (1).

Along with the rising of distributed energy resources, buildings have transformed from traditional electricity consumer into prosumer (producer and consumer), and efficient energy storage is critical in aiding buildings to absorb more local renewable generation and support more grid-interactive services in near future smart grid. Currently available electricity storage technologies have been reviewed and compared based on their lifetime, roundtrip efficiency, and energy density [12] [13]. For instance, Li-ion and Zn-air batteries have exceptionally high energy density and are very promising technologies for building application, but they are still costly to scale up for transmission level deployment. On the other hand, pumped-hydro energy storage (PHS) and underground compressed air energy storage (CAES) are large-scale technologies capable of discharge times of tens

of hours and capacities up to 1GW, e.g. PHS accounts for more then 90% of installed storage capacity and has the longest lifetimes, but they are dependent on suitable topographical conditions and have relatively lower overall efficiency. To overcome the disadvantage of PHS or CAES and address the need for dispatchable high-roundtrip efficiency energy storage, the concept of modular pumped hydro storage (mPHS) is patented [14] and prototyped as Ground Level Integrated Diverse Energy Storage (GLIDES) in Oak Ridge National Laboratory. GLIDES could be treated as combination of PHS and CAES [15], but it uses air pressure in vessel to create high water head instead of lifting water body in conventional PHS, and it uses generally high efficient hydraulic machinery (water pump/turbine) instead of gas compressor/turbine as in conventional CAES. In summary, GLIDES has several advantages: 1) it can be installed at ground level or below, basically anywhere that can structurally support of pressure vessels; 2) it has the ability to integrate a diverse range of low grade heat sources and use the waste heat to boost power generation efficiency in discharging process; 3) it's scalable which makes it possible to be allocated and utilized at grid-scale or equipped for smart buildings for behind-meter applications. Some other recently proposed medium- to large-scale electricity storage technologies include Pumped-Thermal Electricity Storage and Liquid-Air Energy Storage [16].

Since GLIDES technology is moving towards commercialization at current stage, the research roadmap on GLIDES from our team is summarized from the following phases: 1) concept proof and thermodynamic simulation. The concept is introduced [17], and theoretical results are derived from a transient, analytical, physics-based thermodynamic model used for system design and configuration [18]. Experimental thermodynamic performance of the first GLIDES proof-of-concept prototype is reported based on a calibrated/validated physics-based simulation model [19]. 2) market revenue estimation and techno-economic analysis. The first volume-control based operation model of GLIDES is proposed [20] to quantify and estimate its market potential in four ISO real-time markets by providing different operating reserves and regulation services. 3) further operation analysis with various use cases. At building level, stochastic operation model of building microgrid equipped with GLIDES is developed considering uncertainties from solar radiation and electricity load [21] and solved using sample average approximation. Then at community level, GLIDES is assumed as price maker or leader in local energy transaction market and community buildings are followers [22]. Bilevel Stackelberg model is formulated to show revenue potential of GLIDES in local energy trading game. The Kriging surrogate model is trained aiming to provide a more general and efficient capacity planning model for charging station with GLIDES as energy storage [15] and the cost performance of GLIDES and battery storage are compared for this use case. For transmission level application, the integrated operation of GLIDES with run-of-river hydro power plants is under developing and the waste heat from transformer at switch yard is assumed to be utilized by GLIDES. 4) alternative improvement and cost reduction opportunities. Instead of air in vessel, the mixture of CO_2 and N_2 is explored as alternative condensable gas to increase the energy density of GLIDES and the optimal mixture composition is determined by simulation [23]. Various materials for pressure vessels, like steel vessel, carbon fiber vessel, pipe segments and underground pressure reservoirs are analyzed in [24] for cost reduction purposes.

In this research, the waste heat utilization ability of GLIDES is simulated and then its thermal-electricity coupled operation is modeled for building application, where CCHP is assumed as thermal source. The organization of this research is as follows. The configuration for GLIDES to utilize waste heat is introduced briefly in Section 2, followed by a simplified simulation to simulate transient air/water status inside vessel with waste heat; in Section 3, coupled thermal energy and electricity optimization via GLIDES is developed for a smart building; three different cases are conducted for experiments in Section 4 with comparison results. Finally, conclusions are drawn in Section 5.

2. GLIDES Configurations

A typical GLIDES system consists of a liquid storage, pressure vessel(s) (pre-pressurized with the working gas), hydraulic motor/pump and turbine/generator, see Figure 1. In charging process, electricity will drive the motor to pump liquid (e.g. water, oil, etc.) from liquid reservoir to the pressure vessel(s) until certain gas pressure is reached (less than the vessel's maximum allowable pressure). To recover the stored energy, the now high-head water will be pushed by high pressure gas through the hydraulic turbine (e.g. pelton turbine) which spins an electrical generator to re-generate electricity. In this process, the gas pressure/temperature drops along with its expansion, internal energy is converted to hydro power.

To evaluate the performance and work loss in the polytropic process, three different configurations of GLIDES (Figure 2) have been proposed and simulated in previous study [18]. Under base configuration, the work loss due to thermal loss in non-isothermal compression/expansion could be calculated by the area difference under air pressure-liquid volume curves for charging and discharging. The results in [18] show that base configuration has 90% indicated efficiency (ratio of work output and work input) and 66% electric round-trip efficiency (ratio of electrical output and input).

GLIDES has the capability of charging by pumping liquid into the pressure vessel from the bottom, or sprayed into the vessel from the top by a second circulation pump. In configuration 2, it aims to leverage the orders-of-magnitude difference in thermal capacitance between gas and liquid by recirculating the liquid in a secondary loop and spraying it over the gas during charging and discharging. Because of larger thermal capacity of the

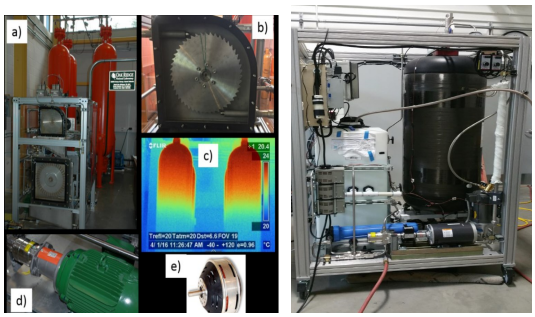

(a) first-generation (b) second-generation

FIGURE 1: Prototypes of first (left figure, material: conventional steel) and second generation GLIDES (right figure, material: carbon fiber)

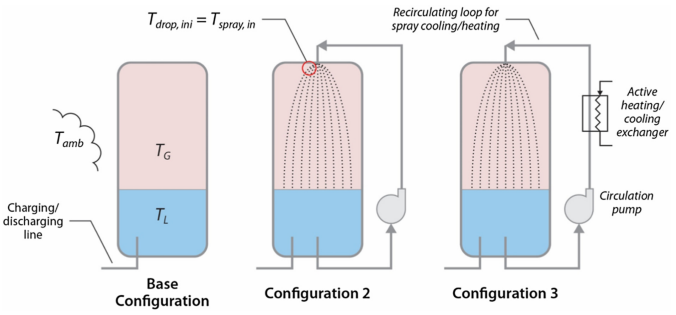

FIGURE 2: Alternative configurations of GLIDES to integrate thermal source

liquid, the liquid temperature remains almost constant, thus the liquid is cooler than the gas (provides cooling) during compression and warmer than the gas (provides heating) during expansion. A noticeable decrease of lost work in two separate near-isothermal processes of compression and expansion is observed, with 96% indicated efficiency and 70% electric round-trip efficiency, reported in previous study [18]. In configuration 3, a thermal exchanger is added downstream of the spray pump to utilize any available waste heat to further enhance the effect of spray warming/cooling during gas expansion/compression. Because of the additional thermal energy, more hydraulic work could be extracted from the system than was stored via the pump. Depending on different heat source temperatures 50 °C, 70 °C, 90 °C, indicated efficiency is boosted to 103%, 107%, 112%, and electric round-trip efficiency becomes 75%, 78% and 82%, reported in [18]. Low grade waste heat sources qualified for GLIDES could be as low as 30-50°C (e.g., from HVAC condensers or cooling towers in building application), medium-temperature heat (50-90 °C, e.g., from solar thermal receivers or combined heat and power, geothermal) or as high as 95-120 °C (e.g., from transformer oil in hydropower plants).

2.1. Simplified Simulation

A very detailed and elaborated simulation of GLIDES with waste heat has been studied in our previous work [18]. However, it is impractical to couple this detailed model to an operational decision model for GLIDES due to the computation burden caused by its complex nonlinear behavior. To develop a tractable operation model, a simplified model was developed first based on configuration 3 in Figure 2. In discharging process, a small liquid stream is diverted from discharging liquid flow and pumped upwards by the circulation pump, on which path, it will be heated up by heat exchanger and then sprayed from the top of the vessels to compensate/boost air pressure in discharging.

The simulation equations are explained as follows. The number of moles of air inside the GLIDES vessel, N, is calculated by

$$N = \frac{M_{air}}{28.965} \tag{1}$$

M_{air} is the mass of air in GLIDES and is calculated from the initial gas properties. For simplicity, it is assumed that the temperature of the waste heat is constant in the heat exchanger. The maximum heat that can be transferred to the circulated GLIDES water can then be calculated by

$$Q^i_{max} = -1 \cdot \dot{m} \cdot \Delta t \cdot C_w \cdot (T^i_{wo} - (T_{WH} - 10)) \tag{2}$$

Where Δt is the simulation time step with index i, $\dot{m}$ is the mass flowrate of the circulated (spray) GLIDES water, T_{WH} is the temperature of the waste heat, T^i_{wo} is the temperature of water at the outlet (bottom) of GLIDES vessel, and C_w is the specific heat of the water. Actual absorbed heat by water flow Q^i_{WH} should be bounded by $Q^i_{WH} \leq Q^i_{max}$ The temperature of the spray T^i_{top} entering into the top of the GLIDES vessel is calculated by

$$T^i_{top} = \frac{Q^i_{WH}}{\dot{m} \cdot \Delta t \cdot C_w} + T^i_{wo} \tag{3}$$

The temperature of the spray T^i_{bot} right before it reaches the water inside the GLIDES vessels is calculated by eq. (4). We define $\alpha \propto h_a \cdot \frac{m}{\rho} \cdot L_a$ as a coefficient. h_a is heat transfer constant between air and sprayed water, $\frac{m}{\rho}$ is the volume of sprayed water. L_a is the distance sprayed water traveled before it reaches water surface in vessel. T^i_{air} is air temperature inside GLIDES.

$$T^i_{bot} = T^{i-1}_{air} + \alpha \cdot (T^i_{top} - T^i_{air}) \tag{4}$$

Then the heat Q^i_{air} transferred to the air of GLIDES can be calculated by eq. (5), and air temperature T^i_{air} is updated by the first law in eq. (6). P^i and V^i are pressure and volume of air in GLIDES, respectively. Q^i_{aw} and Q^i_{ao} are heat transfer from the air inside GLIDES to water inside GLIDES and to ambient air outside of GLIDES, which can be calculated by eq. (7) and (8), respectively. T^i_{wo} is the temperature of the water inside GLIDES. C_v is the specific heat of air. U_{aw} and U_{ao} are heat transfer constant, A_{aw} and A^i_{ao} are the contact areas.

$$Q^i_{air} = \dot{m} \cdot \Delta t \cdot C_w \cdot (T^i_{top} - T^i_{bot}) \tag{5}$$

$$T^i_{air} = \frac{Q^i_{air} - P^{i-1} \cdot (V^i - V^{i-1}) - Q^i_{aw} - Q^i_{ao}}{M_{air} \cdot C_v} + T^{i-1}_{air} \quad (6)$$

$$Q^i_{aw} = U_{aw} \cdot A_{aw} \cdot (T^i_{air} - T^i_{wo}) \quad (7)$$

$$Q^i_{ao} = U_{ao} \cdot A_{ao} \cdot (T^i_{air} - T_{amb}) \quad (8)$$

Redlich-Kwong equation of state is then used to update the air pressure inside the vessel; see eq. (9) and (10) where V_m is the molar volume of air inside the vessel.

$$P^i = \frac{8314 \cdot T^i_{air}}{V_m - 0.02541} - \frac{15.989}{V_m \cdot (V_m + 0.02541) \cdot \sqrt{T^i_{air}}} \quad (9)$$

$$V_m = \frac{V^i}{N} \quad (10)$$

At last, temperature of water inside GLIDES is updated by eq. (11). M^i_w is the mass of water inside GLIDES.

$$T^{i+1}_{wo} = \frac{M^i_w \cdot T^i_{wo} + \dot{m} \cdot \Delta t \cdot T^i_{bot}}{M^i_w + \dot{m} \cdot \Delta t} + \frac{Q^i_{aw}}{M^i_w \cdot C_w} - \frac{Q^i_{wo}}{M^i_w \cdot C_w} \quad (11)$$

Q^i_{wo} is the heat transfer from water inside GLIDES to ambient air outside of GLIDES, which can be calculated by eq. (12), Where U_{wo} is heat transfer constant, A^i_{wo} is the contact area.

$$Q^i_{wo} = U_{wo} \cdot A^i_{wo} \cdot (T^i_{wo} - T_{amb}) \quad (12)$$

Since the charging process could be treated as an isothermal process by using water spray charging, only discharging is considered here. Parameter settings for the simulation are: Δt =1s, T_{amb}=298.15 °K, T_{WH}=343.15 °K, C_w=4.180 kJ/kg·k, C_v=0.717 kJ/kg·k, M_{air}=46.745 kg, $\dot{m}$ = 0.2 kg/s, $\dot{m}_{dis}$=0.583 kg/s, U_{aw}=0.01 kW/m^2·k, U_{ao}=0.005 kW/m^2·k, U_{wo}=0.18 kW/m^2·k. The radius of the pressure vessel r=0.252 m, the height of the pressure vessel L=2.5 m. Initial air volume is 0.3125 m^3, and initial air pressure is 128 bar. The initial air and water temperature are 298.15 °K. The thickness of the pressure vessel wall is 0.02 m. Finally, the maximum allowable air pressure is 132 bar, and the minimum air pressure is 77 bar. The results of the simulation using the above parameters are shown in Figure 3, Figure 4, and Figure 5. Figure 3 shows the pressure-volume and the air temperature during the discharging process with additional waste heat. The air temperature initially increases rapidly from room temperature and then slowly approaches 55 °C. Meanwhile, the air pressure increases initially then slowly decreases as water is discharged from the vessel. To compare the pressure-volume relationship with and without waste heat, Figure 4 is plotted. As shown in Figure 4, without waste heat, the air temperature drops to about 16 °C, mostly due to the boundary work. The area between the two air pressure curves is the additional electricity work converted from added thermal energy. After the water in the GLIDES, the vessel is fully discharged, the heat transfer with ambient dominates. In Figure 5, the air pressure, air temperature, and water temperature are all plotted for the full discharging and the following idle time are plotted against elapsed time.

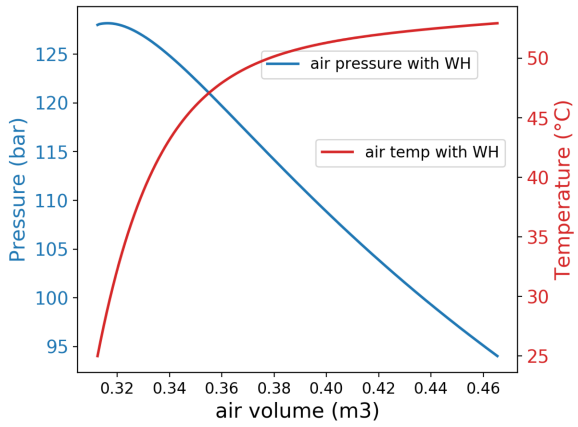

FIGURE 3: Air pressure-volume diagram with waste heat (WH)

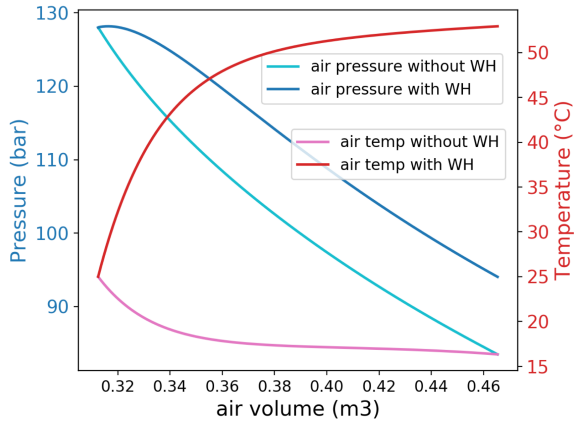

FIGURE 4: Pressure-volume comparison with/without waste heat

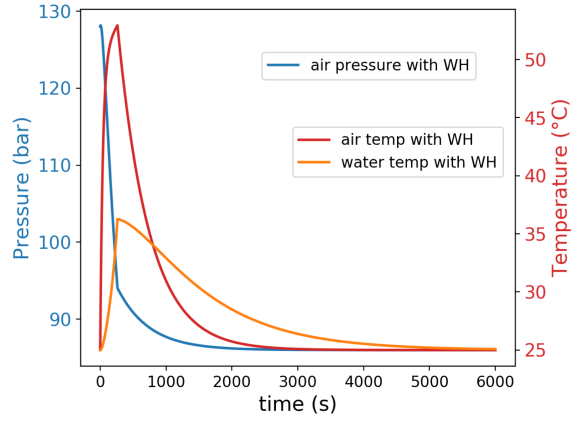

FIGURE 5: Transient pressure and temperature inside vessel with waste heat

3. Power Augmentation of GLIDES

Besides the simplified simulation on demonstrating its waste heat integration ability, an optimization model is developed in this section for power augmented operation of GLIDES. A building application is considered here for illustration purposes and the thermal energy from CCHP system is used as heat input source for GLIDES. It is assumed the building is equipped with a solar panel, CCHP system, thermal energy storage and GLIDES electricity storage. The overall scheme of considered building energy system is shown in Figure 6. A typical CCHP usually consists of a power generation unit (PGU) producing electricity, a heat recovery system coupled with PGU to recover waste thermal energy, an auxiliary boiler to compensate the shortage of thermal energy, an absorption chiller and a heating exchanger as cooling and heating components [6] [25]. All the variables and parameters defined in the proposed operation model are summarized in Table 1 and Table 2.

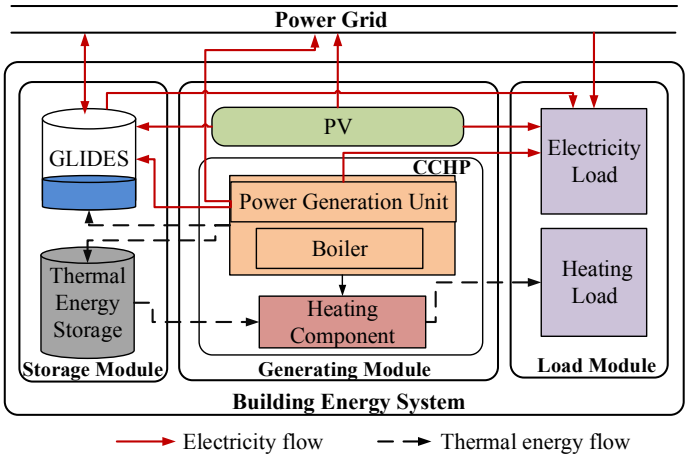

FIGURE 6: Overall scheme and energy flow in a smart building equipped with GLIDES

The objective of thermal-electricity coupled optimization model is to minimize the total operation cost (OC) of a smart building in one day, which consists of electricity purchasing cost, electricity selling profit and fuel cost in Eq.(13).

$$\min OC = \sum_t (eb_t \cdot Pb_t - es_t \cdot Ps_t) + (fP_t + fB_t) \cdot Pf_t \quad (13)$$

Electricity load is balanced in Eq.(14), where PGU power generation, purchased electricity, solar power, electricity discharged from GLIDES are at left hand, and sold electricity to power grid, charged electricity are at right hand side with electricity demand.

$$eu_t + eb_t + er_t + ed_t = EL_t + es_t + ec_t \quad (14)$$

Solar power generation directly depends on solar panel area, radiation level and generating efficiency, which can be estimated

TABLE 1: Parameter notations for the operation model

$t, \Delta t$	Index for time step, period length (15 minutes)
Pb, Ps, Pf	Electricity purchasing, selling price, fuel price
EL, HL	Electricity demand, heating load
SP, SB	Size of PGU, boiler in CCHP
a, b	Fuel-to-electricity conversion coefficient of PGU
SR, Sol_t	Size of solar panel, solar radiation level
ST, SV	Size of thermal storage, pressure vessel of GLIDES
Q_0, V_0, P_0	Initial thermal level, initial liquid, pressure level
$\underline{V}, \overline{V}$	Minimum, maximum liquid volume level in GLIDES
$\underline{\theta}_c, \underline{\theta}_d$	Min coef. of charging, discharging of thermal storage
$\overline{\theta}_c, \overline{\theta}_d$	Max coef. of charging, discharging of thermal storage
$\underline{\alpha}_c, \underline{\alpha}_d$	Min coefficient of charging, discharging of GLIDES
$\overline{\alpha}_c, \overline{\alpha}_d$	Max coefficient of charging, discharging of GLIDES
η_U, η_O	Thermal generating efficiency of PGU, boiler
η_Q, η_H	Efficiency of thermal storage, heating component
η_P, η_M	Efficiency of pump, motor of GLIDES
η_T, η_G	Efficiency of hydro turbine, generator of GLIDES

in Eq.(15).

$$er_t \leq SR \cdot Sol_t \cdot \eta_V \cdot \Delta t \quad (15)$$

Fuel consumed by boiler and PGU in the CCHP are limited by their maximum capacities in Eq.(16) and Eq.(17). Electricity generated by PGU is calculated based on the fuel it consumes and its fuel-to-electricity conversion coefficient in Eq.(18).

$$fB_t \leq SB \quad (16)$$

$$fP_t \leq xU_t \cdot SP \quad (17)$$

$$eu_t \leq (fP_t - b \cdot xU_t)/a \quad (18)$$

In Eq.(19), at right side, thermal energy generated by boiler and waste heat recovered from PGU when generating power are then provided to heating component instantly or stored in thermal storage for later use or absorbed by GLIDES to augment its power generation. Heating load are then satisfied in Eq.(20).

$$qPH_t + qPS_t + qWH_t \leq \eta_U \cdot fP_t + \eta_O \cdot fB_t \quad (19)$$

$$(qPH_t + qSH_t) \cdot \eta_H = HL_t \quad (20)$$

Operating constraints for thermal energy storage are from Eq.(21) to Eq.(26). Stored thermal energy level is determined by charging/discharging activities in Eq.(23). Charging rate is limited by available thermal energy from CCHP in Eq.(24), and discharging rate determines the thermal energy transferred from thermal storage to heating components in Eq.(25). Meanwhile, thermal energy level at the end time step qS_T is required to be

TABLE 2: Variable notations for the operation model

eb, es	Purchased electricity, sold electricity amount
fP, fB	Fuel consumed by PGU, by boiler in CCHP
er, eu	Solar power, power generation by PGU
qPH, qPS	Thermal from CCHP to heating component, to storage
qSH	Thermal from storage to heating component
qWH, q	Available heat for GLIDES, absorbed heat by GLIDES
ec, ed	Electricity charged to, discharged from GLIDES
xu, qS	ON/OFF status of PGU, thermal storage energy level
qc, qd	Charging, discharging rate of thermal storage
xc, xd	Binary charging, discharging of thermal storage
vc, vd	Charging, discharging volumetric flow rate of GLIDES
v, p	Liquid volume level, air pressure level in GLIDES
xp, xg	Binary status of pumping, generating mode of GLIDES

equal as initial level Q_0.

$$xc_t + xd_t \leq 1 \tag{21}$$
$$qS_t \leq ST \tag{22}$$
$$qS_t - qS_{t-1} = (qc_t - qd_t) \cdot \Delta t \tag{23}$$
$$ST \cdot \underline{\theta}_c \cdot xc_t \leq qc_t \leq qBS_t \cdot \eta_Q \leq ST \cdot \overline{\theta}_c \cdot xc_t \tag{24}$$
$$ST \cdot \underline{\theta}_d \cdot xd_t \leq qSH_t/\eta_Q \leq qd_t \leq ST \cdot \overline{\theta}_d \cdot xd_t \tag{25}$$
$$qS_T = Q_0 \tag{26}$$

Constraints for the liquid volume control in GLIDES are formulated in Eq.(27) – (32). The liquid volume level should be kept between the permitted lowest level and its maximum level in Eq.(28) and is determined by charging/discharging activities in Eq.(29). The volumetric flow rate in charging and in discharging the process cannot exceed the range of the lowest and highest levels in Eq.(30)-(31). Meanwhile, liquid volume level in the vessel at last time step v_T is required to be same as initial level V_0.

$$xp_t + xg_t \leq 1 \tag{27}$$
$$\underline{V} \leq v_t \leq \overline{V} \tag{28}$$
$$v_t - v_{t-1} = vc_t - vd_t \tag{29}$$
$$xp_t \cdot \Delta t \cdot \underline{\alpha}_c \cdot \overline{V} \leq vc_t \leq xp_t \cdot \Delta t \cdot \overline{\alpha}_c \cdot \overline{V} \tag{30}$$
$$xg_t \cdot \Delta t \cdot \underline{\alpha}_d \cdot \overline{V} \leq vc_t \leq xg_t \cdot \Delta t \cdot \overline{\alpha}_d \cdot \overline{V} \tag{31}$$
$$v_T = V_0 \tag{32}$$

The liquid-to-power constraints are in Eq.(33)-(34) where the flow power generation is determined by its liquid flow rate and head pressure.

$$ec_t \cdot \eta_P \cdot \eta_M = vc_t \cdot p_t \cdot 1/3600 \tag{33}$$
$$ed_t = \eta_T \cdot \eta_G \cdot vd_t \cdot p_t \cdot 1/3600 \tag{34}$$

Constraints related to external thermal energy in Eq.(35)-(38) are based on the developed simplified simulation model in Section 2.2. q_t is the thermal energy absorbed by air inside GLIDES. The maximum available thermal energy Q_{WH} is calculated by Eq.(2). Since we only consider adding waste heat during discharging, $q_t = 0$ if $xg_t = 0$. To further reduce the computational burden of operation model, water temperature in GLIDES is approximately treated as constant room temperature 25 °C and the heat transfer is neglected, then Eq.(36) is transformed based on Eq.(6) in the simplified simulation model, T_{amb} is a constant room temperature, $T_{air,t}$ is air temperature inside GLIDES which is also a variable in optimization model with initial room temperature. M_{air} is the mass of air in GLIDES. C_v is the specific heat of air. Eq.(37)-(38) are adopted from Eq.(9) - (10) in the simplified simulation model. N is the number of moles of the air inside GLIDES. $V_{m,t}$ is the molar volume of the air. Meanwhile, the air temperature inside vessel of GLIDES at the end of operation $T_{air,T}$ is also required to be same as room temperature by Eq.(39). Note that, the index i in simplified simulation model is 1 second sampling step, and the time index t in operation model here is a 15 minutes decision period.

$$q_t \leq xg_t \cdot \min\{qWH_t, Q_{WH}\} \tag{35}$$
$$T_{air,t} = xp_t \cdot (T_{amb} - T_{air,t-1}) + T_{air,t-1} + \frac{q_t - p_{t-1} \cdot vd_t}{M_{air} \cdot C_v} \tag{36}$$
$$V_{m,t} = \frac{SV - v_t}{N} \tag{37}$$
$$p_t = \frac{8314 \cdot T_{air,t}}{V_{m,t} - 0.02541} - \frac{15.989}{V_{m,t} \cdot (V_{m,t} + 0.02541) \cdot \sqrt{T_{air,t}}} \tag{38}$$
$$T_{air,T} = 298.15(K) \tag{39}$$

4. NUMERICAL EXPERIMENTS

Based on the proposed operation model, three case studies are designed in this section to optimize the coupled thermal-electricity operation, and explore the pressure-volume relationship of GLIDES system with or without additional thermal energy. For the sake of simplicity, the temperature of thermal energy provided by CCHP and thermal energy storage is assumed as 353.15 K (80 °C) for all experiments.

- Case 1: No thermal energy or heat is allowed to be utilized by GLIDES storage.
- Case 2: Thermal energy is limited for GLIDES, and is provided based on coordinated operation of CCHP and thermal energy storage.
- Case 3: Thermal energy is assumed to be unlimited for GLIDES.

For the GLIDES system, one pressure vessel with 10 kW rated power and 8 hours of storage time is assumed here. Given the power and energy capacity, allowable pressure range, the required storage volume and maximum liquid volume in pressure vessel can be derived [20]. The detailed parameter settings of GLIDES are listed in Table 3. Besides GLIDES, the parameters

(e.g. capacity, efficiency) of other energy systems for studied building are listed in Table 4. Prices in Figure 7 including electricity purchasing price, selling price ($0.00367/kWh) and fuel price ($0.027/kWh) are obtained from Ref [25]. In Figure 8, 15-minute electricity and thermal load is scaled based on smart meter data of a residential building in a typical January day [21], solar radiation data for the same location is also adopted [26].

TABLE 3: Parameter settings for the GLIDES system

Parameter	$\overline{P}$ (kpa)	$\underline{P}$	$\overline{V}$ (m^3)	$\underline{V}$	SV	V_0	P_0
Value	13000	7000	35.897	0	89.072	17.948	8766.498
Parameter	η_P,η_M	η_T,η_G	$\overline{\alpha}_c$,$\overline{\alpha}_d$	$\underline{\alpha}_c$,$\underline{\alpha}_d$	–	–	–
Value	0.9,0.9	0.9,0.9	0.25	0.083	–	–	–

TABLE 4: Parameter settings for other energy systems

Parameter	SR (m^2)	SP (kW)	SB (kW)	ST (kW)	η_V	η_U	η_O
Value	7.5	50	50	50	0.25	0.51	0.9
Parameter	η_Q	η_H	$\overline{\theta}_c$,$\overline{\theta}_d$	$\underline{\theta}_c$,$\underline{\theta}_d$	a	b	Q_0
Value	0.8	0.85	0.25, 0.25	0.05, 0.05	2.97	11.66	10

FIGURE 7: Electricity purchasing, selling prices and fuel price

Since thermal energy is not allowed as input for GLIDES in case 1, the added heat is therefore 0 in Figure 9. At beginning, liquid is continuously pumped into pressure vessel of GLIDES system in the charging process between hour 1-9 which are non-peak price hours in Figure 7. Accordingly, air pressure increases along with rising liquid level in the vessel. However, air temperature inside vessel stays the same in the charging process. This is because liquid (eq. water here) has larger thermal capacity and

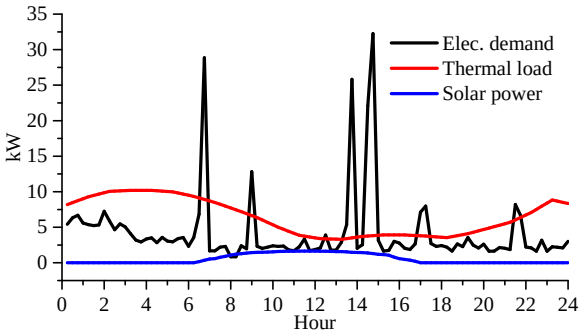

FIGURE 8: Electricity demand, thermal loads and available solar power

its temperature remains almost constant as initial room temperature 25 °C. Thus, the cooler water spray charging from the top of vessel by second circulation pump prevents air temperature from rising and keeps the charging process as isothermal process, as explained in Section 2.1. Then, in electricity price peak around hour 10-20, liquid level in Figure 9 shows GLIDES discharged for most of the time to satisfy electricity load. In the discharging process, gas expands along with falling liquid level and air temperature start to drop below ambient temperature due to the boundary work. Air temperature dropping speed depends on liquid discharging speed, for instance, it drops rapidly to as low as 8 °C around hour 18 and similarly, it is then rewarmed quickly by now warmer water spray (25 °C) charging from top in next time step (15 minutes). Note that, the liquid level inside vessel at the end of operation is required to be equal to initial level for all cases, and the final operating cost is $15.5 under case 1.

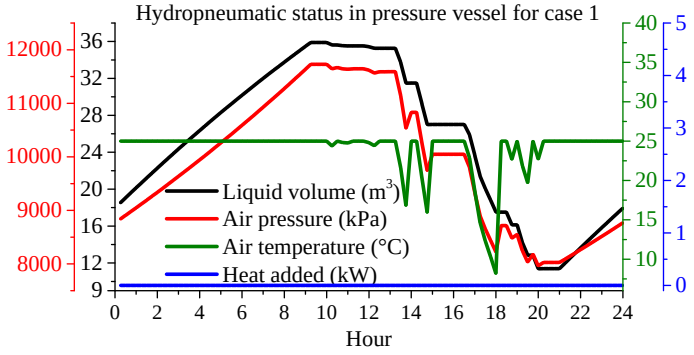

FIGURE 9: Hydropenumatic status in GLIDES vessel for study case 1

In case 2, thermal energy could be provided to GLIDES from CCHP and thermal storage. The charging/discharging pattern shown by liquid volume level in Figure 10 is similar to case

1 but without several idle periods in Figure 9, and GLIDES is fully discharged to zero around hour 20. It is interesting that additional heat is added to GLIDES only in discharging process and just enough to make discharging process also a isothermal process (constant air temperature in Figure 10) as charging, which means, the work loss in non-isothermal expansion is compensated additional thermal energy. The operating cost with limited thermal energy in case 2 is $14.9, about a moderate 3.8% improvement on the comparing with case 1.

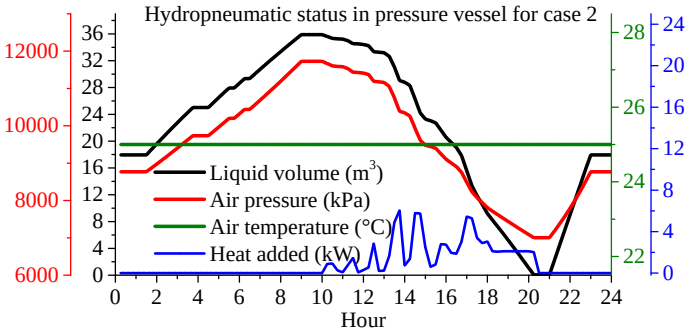

FIGURE 10: Hydropenumatic status in GLIDES vessel for study case 2

For an ideal case 3, heat is assumed to be always available for GLIDES and not depends on CCHP and thermal storage. With the same discharging liquid flow rate, the power generation amount of GLIDES could be boosted indicated by the liquid-to-power generation Eq.(33)-(34). In the three obvious spikes on "Heat added" curve in Figure 11, the strategy is upraise pressure to a high level by adding heat for a short time period, it will then generate needed power with a very small discharging flow rate and thus preserve more liquid level for later use. Subsequently, in the electricity price peak hours or the long discharging process around hour 10-20, heat is added continuously to boost power generation. With additional heat, it is shown that pressure drops much slower in case 3 than case 1 and case 2 at same liquid level. For instance, air pressure is around 8,000 kPa in case 3 at hour 20 where liquid level is almost zero, whereas for the same situation in case 2, the pressure is around minimum level 7,000 kPa when liquid is fully discharged out. The steep dropping of air temperature around hour 5, hour 7, and hour 21 are mostly due to the spray charging from top of vessel by circulating constant room temperature water from bottom of the vessel. The water body remains almost constant temperature 25 °C as explained before and is now much cooler than air, which will cool down air rapidly. The operating cost is $13.5 in case 3, about 12.9% improvement comparing with case 1.

Thermal energy level in thermal storage are shown in Figure 12 for all cases. It is seen that thermal storage stays idle all the

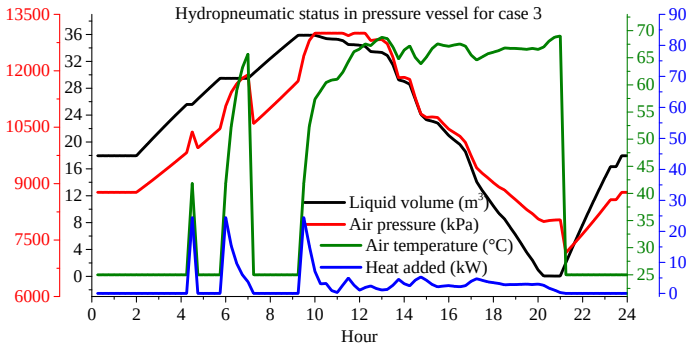

FIGURE 11: Hydropenumatic status in GLIDES vessel for study case 3

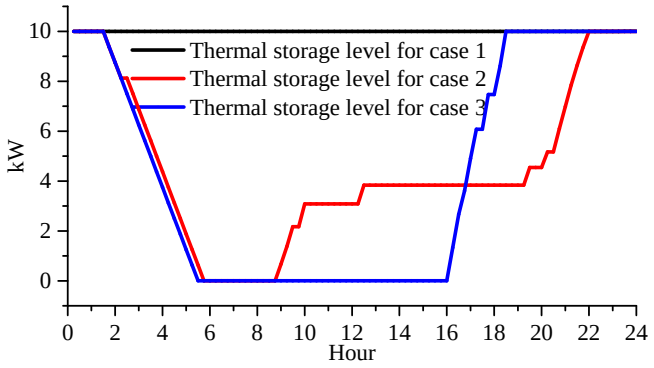

FIGURE 12: Stored thermal energy level in thermal storage for studied cases

time in case 1, this is mainly because GLIDES is not allowed to utilize heat and thermal load could be directly satisfied by heat generated from boiler and PGU. Overall, in case 1, it is not cost efficient to use thermal storage due to its efficiency loss in the operating cycle. On the other hand, Thermal storage has similar storage level pattern for at case 2 and case 3 in Figure 12, where it if fully discharged at the beginning to satisfy the relatively higher thermal load before hour 6 in Figure 8. Then CCHP starts to generate more heat, part of it is added to GLIDES shown by "Heat added" curve in Figure 10 and Figure 11, another part is used to recharge thermal energy to initial storage level.

5. CONCLUSION

In this research, the ability of GLIDES in utilizing available heat source in discharging process to augment power generation is mainly focused. After reviewing several configurations and its efficiency improvement from detailed simulations in our previous research, a simplified simulation model is developed for the purpose of being able to integrate with operation model later. The coupled air pressure, air temperature and water tem-

perature inside pressure vessel are then simulated and compared with/without heat source in a full discharging process. Based on a smart building application, the operation model of GLIDES incorporating heat input from CCHP and thermal energy storage is built and the results are illustrated for three designed study cases. It is shown that, in coordinated operation, GLIDES tends to just compensate gas thermal loss by optimally control heat input and make the whole operation as isothermal process, a cost saving percentage 3.8% is observed for one day operation. While heat source is unlimited, it can be used to boot air pressure instead of discharging more liquid volume for the same amount of power generation. This is beneficial in preserving liquid volume peak demand and maximum cost saving percentage 12.9% is reached in this case.

REFERENCES

[1] U.S. Energy Information Administration, 2019. U.S. total energy production and consumption. https://www.eia.gov/todayinenergy/detail.php?id=43515.

[2] Yang Chen, 2018. Uncertainty-Aware Transactive Operation Decisions for Grid-Friendly Building Clusters. https://hdl.handle.net/10027/22722, 8.

[3] Wu, D., Han, Z., Liu, Z., and Zhang, H., 2019. "Study on configuration optimization and economic feasibility analysis for combined cooling, heating and power system". *Energy Conversion and Management,* ***190***, pp. 91 – 104.

[4] Maraver, D., Sin, A., Sebastián, F., and Royo, J., 2013. "Environmental assessment of cchp (combined cooling heating and power) systems based on biomass combustion in comparison to conventional generation". *Energy,* ***57***, pp. 17 – 23.

[5] Yang, G., Zheng, C., and Zhai, X., 2017. "Influence analysis of building energy demands on the optimal design and performance of cchp system by using statistical analysis". *Energy and Buildings,* ***153***, pp. 297 – 316.

[6] Dai, R., Hu, M., Yang, D., and Chen, Y., 2015. "A collaborative operation decision model for distributed building clusters". *Energy,* ***84***, pp. 759 – 773.

[7] Afzali, S. F., and Mahalec, V., 2018. "Novel performance curves to determine optimal operation of cchp systems". *Applied Energy,* ***226***, pp. 1009 – 1036.

[8] Song, X., Liu, L., Zhu, T., Zhang, T., and Wu, Z., 2016. "Comparative analysis on operation strategies of cchp system with cool thermal storage for a data center". *Applied Thermal Engineering,* ***108***, pp. 680 – 688.

[9] Soheyli, S., Shafiei Mayam, M. H., and Mehrjoo, M., 2016. "Modeling a novel cchp system including solar and wind renewable energy resources and sizing by a cc-mopso algorithm". *Applied Energy,* ***184***, pp. 375 – 395.

[10] Bird, T. J., and Jain, N., 2020. "Dynamic modeling and validation of a micro-combined heat and power system with integrated thermal energy storage". *Applied Energy,* ***271***, p. 114955.

[11] Dahash, A., Ochs, F., Tosatto, A., and Streicher, W., 2020. "Toward efficient numerical modeling and analysis of large-scale thermal energy storage for renewable district heating". *Applied Energy,* ***279***, p. 115840.

[12] Gür, T. M., 2018. "Review of electrical energy storage technologies, materials and systems: challenges and prospects for large-scale grid storage". *Energy Environ. Sci.,* ***11***, pp. 2696–2767.

[13] Koohi-Fayegh, S., and Rosen, M., 2020. "A review of energy storage types, applications and recent developments". *Journal of Energy Storage,* ***27***, p. 101047.

[14] Momen, A. M., Kyle, J., Abdelaziz, O. A., Vineyard, E. A., Abu-heiba, A., and Odukomaiya, A. O., 2017. "Near isothermal combined compressed gas/pumped-hydro electricity storage with waste heat recovery capabilities". *Current Assignee: UT-Battelle LLC*, p. Patent No. US 2017/0082123 A1.

[15] Chen, Y., Dababneh, F., Zhang, B., Kassaee, S., Smith, B. T., Liu, X., and Momen, A. M., 2019. "Surrogate Modeling for Capacity Planning of Charging Station Equipped With Photovoltaic Panel and Hydropneumatic Energy Storage". *Journal of Energy Resources Technology,* ***142***(5).

[16] Georgiou, S., Shah, N., and Markides, C. N., 2018. "A thermo-economic analysis and comparison of pumped-thermal and liquid-air electricity storage systems". *Applied Energy,* ***226***, pp. 1119 – 1133.

[17] Odukomaiya, A., Momen, A. M., Abu-Heiba, A., Gluesenkamp, K., Abdelaziz, O., and Graham, S., 2015. "Transient Thermofluids Analysis of a Ground-Level Integrated Diverse Energy Storage (GLIDES) System". In ASME 2015 International Mechanical Engineering Congress and Exposition, Vol. 6B, Energy, p. V06BT07A038.

[18] Odukomaiya, A., Abu-Heiba, A., Gluesenkamp, K. R., Abdelaziz, O., Jackson, R. K., Daniel, C., Graham, S., and Momen, A. M., 2016. "Thermal analysis of near-isothermal compressed gas energy storage system". *Applied Energy,* ***179***, pp. 948–960.

[19] Odukomaiya, A., Abu-Heiba, A., Graham, S., and Momen, A. M., 2018. "Experimental and analytical evaluation of a hydro-pneumatic compressed-air Ground-Level Integrated Diverse Energy Storage (GLIDES) system". *Applied Energy,* ***221***(April), pp. 75–85.

[20] Chen, Y., Odukomaiya, A., Kassaee, S., O'Connor, P., Momen, A. M., Liu, X., and Smith, B. T., 2019. "Preliminary analysis of market potential for a hydropneumatic ground-level integrated diverse energy storage system". *Applied Energy,* ***242***, pp. 1237 – 1247.

[21] Chen, Y., Omitaomu, O. A., Hu, M., Kassaee, S., Odukomaiya, A., O'Connor, P., Momen, A. M., Smith, B. T., and

Liu, X., 2019. "Allocation and operation of a hydropneumatic energy storage with building microgrid". In 2019 IEEE Power Energy Society General Meeting (PESGM), pp. 1–5.

[22] Chen, Y., Kou, X., Olama, M., Zandi, H., Liu, C., Kassaee, S., Smith, B. T., Abu-Heiba, A., and Momen, A. M., 2020. Bi-Level Optimization for Electricity Transaction in Smart Community With Modular Pump Hydro Storage, aug.

[23] Abuheiba, A., Ally, M. R., Smith, B., and Momen, A., 2020. "Increasing Compressed Gas Energy Storage Density Using CO 2 –N 2 Gas Mixture". p. 2431.

[24] Kassaee, S., Abu-Heiba, A., Ally, M. R., Mench, M. M., Liu, X., Odukomaiya, A., Chen, Y., King, T. J., Smith, B. T., and Momen, A. M., 2019. "Part 1- techno-economic analysis of a grid scale ground-level integrated diverse energy storage (glides) technology". *Journal of Energy Storage,* ***25***, p. 100792.

[25] Chen, Y., and Hu, M., 2016. "Balancing collective and individual interests in transactive energy management of interconnected micro-grid clusters". *Energy,* ***109***, pp. 1075–1085.

[26] National Renewable Energy Laboratory, 2017. National Solar Radiation Data Base.